

Optical observation of quasiperiodic Heisenberg antiferromagnets in two dimensions

Takashi Inoue and Shoji Yamamoto*

Department of Physics, Hokkaido university, Sapporo 060-0810, Japan

Key words: Quasicrystal, Heisenberg antiferromagnet, Raman scattering, Spin-wave theory

* Corresponding author: e-mail yamamoto@phys.sci.hokudai.ac.jp

We calculate magnetic Raman spectra of Heisenberg antiferromagnets on the two-dimensional Penrose lattice. We follow the Shastry-Shraiman formulation of Raman scattering in a strongly correlated Hubbard system and obtain the second- and fourth-order effective Raman operators. The second-order Raman intensity comes from the E_2 mode, and it is invariant under an arbitrary rotation of polarization vectors. The fourth-order Raman intensities consist of A_1 and A_2 , as well as E_2 , modes and therefore yield strong polarization dependence. In particular, the A_2 mode intensity directly detects the dynamical spin-chirality fluctuations. Employing linearly and circularly polarized lights, we can separately extract every irreducible representation from the observations. We further discuss effects of magnon-magnon interactions on the magnetic Raman scattering. Our theory provides a reasonable explanation for the two-magnon scattering process.

Copyright line will be provided by the publisher

1 Introduction

Since the discovery of quasicrystal [1], quasiperiodic systems have been of much interest. Quasicrystal is characterized by quasiperiodicity, which is a long-range order without translational symmetry and a crystallographically forbidden rotational symmetry. These expect that the physical properties of quasiperiodic systems are quite different from both periodic and amorphous systems. Penrose lattice is one of the most popular two-dimensional quasicrystals. On this lattice, the tight-binding model for noninteracting electrons has been studied. It shows many interesting features such as the confined state [2,3], which is characterized by thermodynamically degenerate states with strictly localized and self-similar wave functions, and multifractal spectrum [4]. Recently, quantum critical behavior has been observed in the quasicrystal $\text{Au}_{51}\text{Al}_{34}\text{Yb}_{15}$ [5]. In this compound, the $4f$ electrons of Yb are strongly correlated, so that investigation of the interplay of the quasiperiodicity and strong correlation is a big issue. On the quasiperiodic systems, strongly correlated electron models have been studied such as Hubbard model [6], Ising model for classical spins [7], and Heisenberg model for quantum spins [8,9]. In this paper, we will study the antiferromagnetic Heisenberg model on the Penrose lattice.

One of the important probes of antiferromagnets is a magnetic Raman scattering. It is an inelastic photon scattering mediated by magnetic excitations. Loudon and Fleury established the standard framework of the two-magnon Raman scattering [10]. For instance, it was used to estimate the exchange interaction constant in the high- T_c superconductor La_2CuO_4 [11]. Theoretically, insulating phase of layered cuprates can be well accounted for quasi-two-dimensional Heisenberg antiferromagnets on the square lattice. Zero-temperature magnetic Raman spectra are calculated by spin-wave theory [12,13,14], exact diagonalization [14], and quantum Monte Carlo method [14]. The magnetic Raman spectrum is also computed in other systems, such as the triangle lattice [15] and the Kagome lattice [16]. Polarization dependence of the magnetic Raman intensity depends on the lattice geometry and the symmetry of the ground state. It provides useful information of magnetic excitations.

Microscopic description of the magnetic Raman scattering is given by Shastry and Shraiman [17,18]. In this formulation, the Loudon-Fleury mechanism is obtained in a second-order perturbation theory. The higher-order perturbation reads beyond the Loudon-Fleury mechanism magnetic Raman scattering, and it includes additional mag-

Copyright line will be provided by the publisher

netic excitations as the spin-chirality terms $\mathbf{S}_i \cdot (\mathbf{S}_j \times \mathbf{S}_k)$ and/or the ring-exchange terms $(\mathbf{S}_i \cdot \mathbf{S}_j)(\mathbf{S}_k \cdot \mathbf{S}_l)$ [19,20]. We will present the Raman intensity profile within and beyond the Loudon-Fleury mechanism on the Penrose lattice Heisenberg antiferromagnets.

2 Model

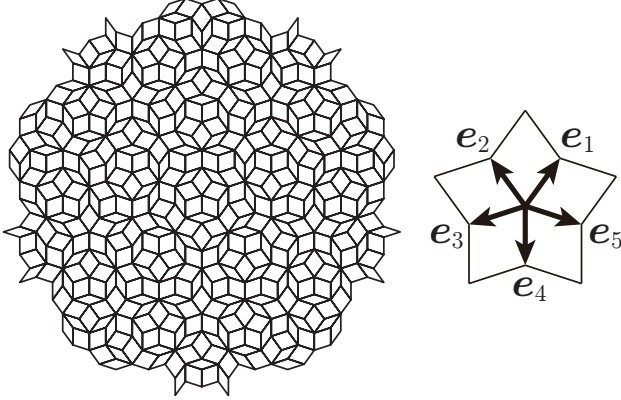


Figure 1 Central patch of the two-dimensional Penrose lattice with fivefold rotational symmetry and its primitive lattice vectors. e_1, \dots, e_5 are projection of the five-dimensional canonical basis vectors, and they satisfy $e_1 + e_2 + e_3 + e_4 + e_5 = \mathbf{0}$.

2.1 Penrose lattice

Figure 1 shows a finite cluster of the Penrose lattice. It is composed of two prototiles: angle $\pi/5$ (thin) and angle $2\pi/5$ (fat) rhombuses. Since the lattice consists of even-number-sided polygons, the Penrose lattice is bipartite. The two-dimensional Penrose lattice is obtained by projection of a five-dimensional hypercubic lattice onto an irrational tilted plane [8], and it holds four independent primitive lattice vectors. Due to the quasiperiodicity, the rank of the Penrose lattice $r = 4$ is larger than the lattice dimension $d = 2$. In this study, we consider open-boundary clusters of the Penrose lattice which hold fivefold rotational symmetry.

2.2 Hamiltonian

We consider the so-called vertex model, where spins are located at vertices of the Penrose rhombus tiling. We consider the nearest-neighbor antiferromagnetic Heisenberg model:

$$H = J \sum_{\langle i,j \rangle} \mathbf{S}_i \cdot \mathbf{S}_j \quad (J > 0) \quad (1)$$

where \mathbf{S}_i is a spin-1/2 operator at site i , and $\langle i, j \rangle$ are pairs of linked vertices of the Penrose lattice.

2.3 Spin-wave theory

We divide the Penrose lattice into two sublattices A and B consisting of N_A and N_B sites, respectively. We introduce bosonic operators by using the Holstein-Primakoff trans-

formation:

$$\begin{aligned} S_i^z &= S - a_i^\dagger a_i \\ S_i^+ &= (2S - a_i^\dagger a_i)^{\frac{1}{2}} a_i \\ S_i^- &= a_i^\dagger (2S - a_i^\dagger a_i)^{\frac{1}{2}} \end{aligned} \quad (2)$$

for $i \in A$, and

$$\begin{aligned} S_j^z &= -S + b_j^\dagger b_j \\ S_j^+ &= b_j^\dagger (2S - b_j^\dagger b_j)^{\frac{1}{2}} \\ S_j^- &= (2S - b_j^\dagger b_j)^{\frac{1}{2}} b_j \end{aligned} \quad (3)$$

for $j \in B$. Expanding the square roots of $1/S$, and keeping terms of $O(S^0)$, spin-wave Hamiltonian is written as

$$\begin{aligned} H_{\text{SW}} = J \sum_{\langle i,j \rangle} & \left[-S^2 + S(a_i^\dagger a_i + b_j^\dagger b_j + a_i b_j + a_i^\dagger b_j^\dagger) \right. \\ & \left. - \left\{ a_i^\dagger a_i b_j^\dagger b_j + \frac{1}{4}(a_i^\dagger a_i a_i b_j + a_i^\dagger b_j^\dagger b_j^\dagger b_j + \text{H.c.}) \right\} \right] \end{aligned} \quad (4)$$

We apply the Wick decomposition for the $O(S^0)$ terms in Eq. (4),

$$\begin{aligned} a_i^\dagger a_i b_j^\dagger b_j & \rightarrow \langle a_i^\dagger a_i \rangle b_j^\dagger b_j + \langle b_j^\dagger b_j \rangle a_i^\dagger a_i - \langle a_i^\dagger a_i \rangle \langle b_j^\dagger b_j \rangle \\ & + \langle a_i^\dagger b_j^\dagger \rangle a_i b_j + \langle a_i b_j \rangle a_i^\dagger b_j^\dagger - \langle a_i^\dagger b_j^\dagger \rangle \langle a_i b_j \rangle \\ a_i^\dagger a_i a_i b_j & \rightarrow 2(\langle a_i^\dagger a_i \rangle a_i b_j + \langle a_i b_j \rangle a_i^\dagger a_i - \langle a_i^\dagger a_i \rangle \langle a_i b_j \rangle) \\ a_i^\dagger b_j^\dagger b_j^\dagger b_j & \rightarrow 2(\langle a_i^\dagger b_j^\dagger \rangle b_j^\dagger b_j + \langle b_j^\dagger b_j \rangle a_i^\dagger b_j^\dagger - \langle a_i^\dagger b_j^\dagger \rangle \langle b_j^\dagger b_j \rangle) \\ a_i^\dagger a_i^\dagger a_i b_j^\dagger & \rightarrow 2(\langle a_i^\dagger a_i \rangle a_i^\dagger b_j^\dagger + \langle a_i^\dagger b_j^\dagger \rangle a_i^\dagger a_i - \langle a_i^\dagger a_i \rangle \langle a_i^\dagger b_j^\dagger \rangle) \\ a_i b_j^\dagger b_j b_j & \rightarrow 2(\langle a_i b_j \rangle b_j^\dagger b_j + \langle b_j^\dagger b_j \rangle a_i b_j - \langle a_i b_j \rangle \langle b_j^\dagger b_j \rangle) \end{aligned} \quad (5)$$

where $\langle \dots \rangle$ denotes the quantum average in the magnon vacuum. Here, we have omitted normal order of the quartic terms and assumed that $\langle a_i^\dagger b_j^\dagger \rangle = \langle a_i b_j \rangle = \langle a_i a_i \rangle = \langle a_i^\dagger a_i^\dagger \rangle = \langle b_j^\dagger b_j^\dagger \rangle = \langle b_j b_j \rangle = 0$ due to the conservation of magnetization. After the decomposition of the quartic terms, we have a quadratic form spin-wave Hamiltonian in real space. Carrying out the Bogoliubov transformation, we can diagonalize the quadratic spin-wave Hamiltonian into

$$H'_{\text{SW}} = \sum_{k=1}^{n_\alpha} \varepsilon_k^{(\alpha)} \alpha_k^\dagger \alpha_k + \sum_{l=1}^{n_\beta} \varepsilon_l^{(\beta)} \beta_l^\dagger \beta_l + E_{\text{GS}} \quad (6)$$

where $\varepsilon_k^{(\alpha)}$ [$\varepsilon_l^{(\beta)}$] is the eigenvalue of the bosonic quasiparticle mode α_k (β_l), n_α (n_β) is the number of the α_k (β_l) modes, and E_{GS} is the ground-state energy.

3 Effective magnetic Raman operator

The magnetic Raman scattering is described by interaction between spin and photon. In this section, we follow a microscopic description of the magnetic Raman scattering, which is first given by Shastry and Shraiman [17, 18, 19, 20], and present effective magnetic Raman operator on the Penrose lattice. First, we consider a strongly correlated single-band Hubbard model:

$$H_{\text{Hb}} = H_U + H_t = U \sum_i n_{i\uparrow} n_{i\downarrow} - \sum_{i,j,\sigma} t_{ij} c_{i\sigma}^\dagger c_{j\sigma} \quad (7)$$

where $c_{i\sigma}^\dagger$ ($c_{i\sigma}$) is the electron creation (annihilation) operator at site i with spin $\sigma = \uparrow, \downarrow$ and $n_{i\sigma} \equiv c_{i\sigma}^\dagger c_{i\sigma}$. t_{ij} is the transfer integral, and $U (> 0)$ is the on-site Coulomb repulsion. Hereafter, we restrict that electron hopping only occurs between nearest-neighbor sites.

The electron-photon coupling can be introduced by the Peierls substitution: $c_{i\sigma}^\dagger c_{j\sigma} \rightarrow c_{i\sigma}^\dagger c_{j\sigma} \exp(\frac{ie}{\hbar c} \int_j^i \mathbf{A} \cdot d\mathbf{r})$, where \mathbf{A} is the photon vector potential. We assume that incoming and outgoing photon wavelengths are much larger than lattice spacing. Then second-quantized vector potential is written as $\mathbf{A} = g_{\text{in}} \mathbf{e}_{\text{in}} \gamma_{\mathbf{k}_{\text{in}}} + g_{\text{sc}} \mathbf{e}_{\text{sc}}^* \gamma_{\mathbf{k}_{\text{sc}}}^\dagger$ where $g_{\text{in}} = \sqrt{\hbar c^2 / \omega_{\text{in}} V}$ and $g_{\text{sc}} = \sqrt{\hbar c^2 / \omega_{\text{sc}} V}$ with volume V . $\omega_{\text{in}}(\omega_{\text{sc}})$, $\mathbf{k}_{\text{in}}(\mathbf{k}_{\text{sc}})$, and $\mathbf{e}_{\text{in}}(\mathbf{e}_{\text{sc}})$ stand for frequency, momentum, and polarization of incident (scattered) photon, respectively. $\gamma^\dagger(\gamma)$ denotes the photon creation (annihilation) operator. Expanding the exponential of the hopping terms, the current operator reads

$$H_c = -\frac{ie}{\hbar c} \sum_{i,j,\sigma} t_{ij} \mathbf{A} \cdot \delta_{ij} c_{i\sigma}^\dagger c_{j\sigma} \quad (8)$$

where δ_{ij} is the vector connecting sites i and j .

Since the Raman process is made of two photons (one photon in, one photon out), we consider second-order terms in \mathbf{A} . We are interested in half-filled ($\sum_\sigma \langle n_{i\sigma} \rangle = 1$) and localized ($U \gg t$) system, H_c and H_t can be treated as a perturbation. In this situation, initial states and final states belong to the ground-state manifold of singly occupied states. The effective Raman operator reads

$$\begin{aligned} \mathcal{R} &= \mathcal{P} H_c \frac{1}{\varepsilon_i - H_U - H_t} H_c \mathcal{P} \\ &= \mathcal{P} H_c \frac{1}{\varepsilon_i - H_U} \sum_{n=0}^{\infty} \left(H_t \frac{1}{\varepsilon_i - H_U} \right)^n H_c \mathcal{P} \quad (9) \end{aligned}$$

where ε_i is the initial-state energy and \mathcal{P} is a projection operator to the spin-1/2 sector. Because of the electron-hole symmetry in the half-filled band, any term of odd n vanishes in Eq. (9). Finally, we convert to electron operators into $S = 1/2$ spin operators using the following projection:

$$\mathcal{P} c_{i\sigma}^\dagger c_{i\sigma'} \mathcal{P} = \frac{1}{2} \delta_{\sigma',\sigma} + \mathbf{S}_i \cdot \boldsymbol{\tau}_{\sigma'\sigma} \quad (10)$$

where $\boldsymbol{\tau}$ is the Pauli matrix.

The second-order perturbation is the lowest nonvanishing order in the Shastry-Shraiman formulation, and it gives the Loudon-Fleury magnetic Raman operator [10]:

$$\mathcal{R}^{(2)} = \sum_{\langle i,j \rangle} \frac{4t^2}{U - \hbar\omega_{\text{in}}} (\mathbf{e}_{\text{in}} \cdot \delta_{ij}) (\mathbf{e}_{\text{sc}}^* \cdot \delta_{ij}) \mathbf{S}_i \cdot \mathbf{S}_j \quad (11)$$

Here, we omit some constants, which does not affect the Raman intensity.

The fourth-order effective magnetic Raman operator, which is the next nonvanishing perturbation at the prefactor $t^4 / (U - \hbar\omega_{\text{in}})^3$, includes the scalar-spin-chirality terms $\mathbf{S}_i \cdot (\mathbf{S}_j \times \mathbf{S}_k)$ and/or the ring-exchange terms $(\mathbf{S}_i \cdot \mathbf{S}_j)(\mathbf{S}_k \cdot \mathbf{S}_l)$. For details about the fourth-order magnetic Raman operator, see Appendix. If the incident photon energy $\hbar\omega_{\text{in}}$ approaches to resonant limit $|U - \hbar\omega_{\text{in}}| \sim t$, higher-order contributions can manifest in Raman intensities.

For theoretical calculations, it is convenient to decompose the polarization dependence of the magnetic Raman spectrum into the irreducible representations (irreps) of the lattice point group. The point group of the Penrose lattice is C_{5v} , polarization dependence of Raman active modes decomposes into two one-dimensional irreps A_1 and A_2 , and one two-dimensional irrep E_2 as follow:

$$\begin{aligned} A_1 &: e_{\text{in}}^x e_{\text{sc}}^{*x} + e_{\text{in}}^y e_{\text{sc}}^{*y} \\ A_2 &: e_{\text{in}}^x e_{\text{sc}}^{*y} - e_{\text{in}}^y e_{\text{sc}}^{*x} \\ E_2^{(1)} &: e_{\text{in}}^x e_{\text{sc}}^{*x} - e_{\text{in}}^y e_{\text{sc}}^{*y} \\ E_2^{(2)} &: e_{\text{in}}^x e_{\text{sc}}^{*y} + e_{\text{in}}^y e_{\text{sc}}^{*x} \quad (12) \end{aligned}$$

The magnetic Raman spectrum is given by Fermi's golden rule:

$$I(\omega) = \sum_n \left| \langle \Psi_n | \mathcal{R} | \Psi_0 \rangle \right|^2 \delta(\hbar\omega - E_n + E_0) \quad (13)$$

where $|\Psi_0\rangle$ is a ground state of the Heisenberg model, $|\Psi_n\rangle$ is excited states, E_0 and E_n are eigenvalues of ground state and excited states, respectively.

4 Results

4.1 Second-order magnetic Raman intensity: Within the Loudon-Fleury mechanism

First, we consider the Raman spectrum within the Loudon-Fleury mechanism. In this section, we use the second-order magnetic Raman operator [Eq. (11)]. Spin operators in Eq. (11) are expanded by the Holstein-Primakoff bosons. In this study, we consider the two-magnon scattering which corresponds to the expansion of the magnetic Raman operator up to the bosonic two-body terms.

In Fig. 2, we give the result of the spin-wave calculation of the two-magnon scattering magnetic Raman intensity within the second-order Raman operator for the $N = 601$ sites cluster of the Penrose lattice. We find

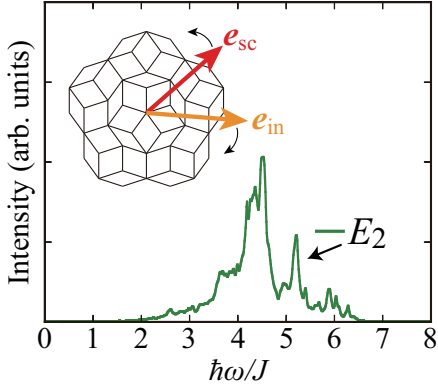


Figure 2 Two-magnon scattering magnetic Raman spectrum of the $N = 601$ sites cluster Penrose lattice Heisenberg antiferromagnet within the second-order magnetic Raman operator. The spectrum comes from the E_2 representation of the C_{5v} point group, and does not depend on the incident and scattered photon polarizations e_{in} and e_{sc}^* .

the second-order Raman intensity comes from the E_2 representation and shows no linear polarization dependence. To understand this depolarization, we set the incident and scattered polarization vectors as

$$e_{in} = (\cos \theta_{in}, \sin \theta_{in}), \quad e_{sc} = (\cos \theta_{sc}, \sin \theta_{sc}) \quad (14)$$

where θ_{in} and θ_{sc} are the angles of the polarization vectors of the incident and scattered photons with respect to the x axis. Under this condition, the E_2 mode Raman spectrum is written as

$$I(\omega, \theta_{in}, \theta_{sc}) = \sum_n \left| \langle \Psi_n | \mathcal{R}_{E_2^{(1)}} \cos(\theta_{in} + \theta_{sc}) + \mathcal{R}_{E_2^{(2)}} \sin(\theta_{in} + \theta_{sc}) | \Psi_0 \rangle \right|^2 \times \delta(\hbar\omega - E_n + E_0) \quad (15)$$

where $\mathcal{R}_{E_2^{(1)}}$ and $\mathcal{R}_{E_2^{(2)}}$ are irreducible decomposed Raman operators of first- and second components of the E_2 representations, respectively. $\mathcal{R}_{E_2^{(1)}}$ and $\mathcal{R}_{E_2^{(2)}}$ are orthogonal to each other, and cross sections of $\mathcal{R}_{E_2^{(1)}}$ and $\mathcal{R}_{E_2^{(2)}}$ are degenerate. Therefore, the E_2 mode Raman spectrum is invariant to polarization angles:

$$I(\omega, \theta_{in}, \theta_{sc}) = \cos^2(\theta_{in} + \theta_{sc}) I_{E_2}(\omega) + \sin^2(\theta_{in} + \theta_{sc}) I_{E_2}(\omega) = I_{E_2}(\omega) \quad (16)$$

where $I_{E_2}(\omega)$ denotes intensity of the E_2 mode.

4.2 Fourth-order magnetic Raman intensity: Beyond the Loudon-Floury mechanism

Next, we calculate the two-magnon Raman intensity of the fourth-order magnetic Raman operator. We consider two polarizations, one is called xx polarization that corresponds to $(\theta_{in}, \theta_{sc}) = (0, 0)$ [Fig. 3(a)], and another

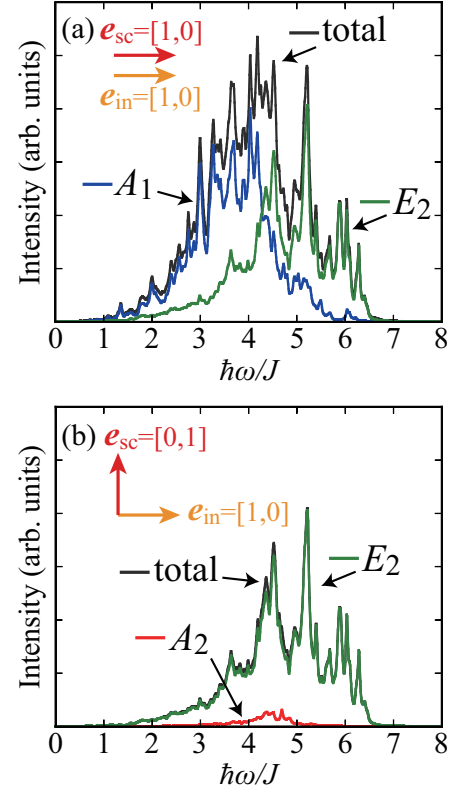


Figure 3 Two-magnon scattering magnetic Raman spectra of the fourth-order magnetic Raman operator on the $N = 601$ sites cluster for xx polarization (a) and xy polarization (b). Sum of all Raman active modes (denoted by “total”) is observed in each polarization in actuality.

is called xy polarization that corresponds to $(\theta_{in}, \theta_{sc}) = (0, \pi/2)$ [Fig. 3(b)]. As shown in Fig. 3, the fourth-order Raman operators yield spectral weight of the A_1 mode in the xx polarization, and the A_2 mode in the xy polarization, as well as the linearly polarization independent E_2 mode. The observed spectra of each polarization are written as $I_{xx}(\omega) = I_{A_1}(\omega) + I_{E_2}(\omega)$ for the xx polarization, and $I_{xy}(\omega) = I_{A_2}(\omega) + I_{E_2}(\omega)$ for the xy polarization. In general, the linear polarization dependence of the fourth-order Raman intensity is given by

$$I(\omega, \theta_{in}, \theta_{sc}) = \cos^2(\theta_{in} - \theta_{sc}) I_{A_1}(\omega) + \sin^2(\theta_{in} - \theta_{sc}) I_{A_2}(\omega) + I_{E_2}(\omega) \quad (17)$$

As shown in Eq. (17), the fourth-order Raman spectrum is observed as combination of irreducible spectra. To extract every irreducible representation from observations, we employ two linearly and one circularly polarized lights. If we only consider linearly polarized lights, we lack degrees of freedom to separate every irreducible representation, so that why circularly polarized light is required. Solving the relations of the polarizations, we can separate every irre-

ducible representation as:

$$\begin{aligned} I_{A_1}(\omega) &= I_{xx}(\omega) - \frac{1}{2}I_{LR}(\omega) \\ I_{A_2}(\omega) &= I_{xy}(\omega) - \frac{1}{2}I_{LR}(\omega) \\ I_{E_2}(\omega) &= \frac{1}{2}I_{LR}(\omega) \end{aligned} \quad (18)$$

where $I_{LR}(\omega)$ is the LR polarization Raman intensity, which LR signifies left circularly polarized incident photon $e_{in} = \frac{1}{\sqrt{2}}(1, i)$ and right circularly polarized scattered photon $e_{sc} = \frac{1}{\sqrt{2}}(1, -i)$.

The fourth-order magnetic Raman spectra include contributions of several magnetic excitations. In particular, the A_2 mode spectrum is intriguing, because it provides a direct observation of dynamical spin-chirality fluctuations. The spin-chirality terms in the fourth-order magnetic Raman operator cancel on the two types of fourth-order-electron-hopping pathways: (1) four-site loop pathway and (2) three-site straight pathway. For example, we consider the two-dimensional periodic lattice with single-site unit cell. This lattice has only two primitive lattice vectors, and it always satisfies the conditions of the spin-chirality-term cancellation. However, this is not the case for the Penrose lattice. Because of the quasiperiodicity, the Penrose lattice has additional primitive lattice vectors and extra pathways of the fourth-order electron hopping, so that the spin-chirality-driven A_2 mode spectrum can survive.

4.3 Effects of magnon-magnon interactions

In this section, we discuss effects of magnon-magnon interactions on the magnetic Raman scattering. We consider small size ($N = 16$) cluster in order to compare spin-wave results with exact spectra obtained by the Lanczös exact diagonalization. In the Lanczös method, the Raman spectrum is obtained from a continued fraction:

$$I(\omega) = -\frac{1}{\pi} \text{Im} \left\{ \langle \Psi_0 | \mathcal{R}^\dagger \frac{1}{\hbar\omega + E_0 + i\eta - H} \mathcal{R} | \Psi_0 \rangle \right\} \quad (19)$$

where η is a small imaginary part added to give a finite damping of the δ -functions.

In the spin-wave calculation, we introduce the magnon-magnon interactions by the configuration interaction (CI) method. We apply the two-magnon excitation CI method in this study. We consider a zero-magnon state $|0M\rangle$ and two-magnon excited states $|2M\rangle$:

$$|0M\rangle = |0\rangle, \quad |2M(k, l)\rangle = \alpha_k^\dagger \beta_l^\dagger |0\rangle \quad (20)$$

where $|0\rangle$ is a magnon-vacuum state. Spin-wave eigenstates are improved as

$$|\Psi_n\rangle_{CI} = c_{0,n}|0\rangle + \sum_{k,l} c_{(k,l),n} \alpha_k^\dagger \beta_l^\dagger |0\rangle \quad (21)$$

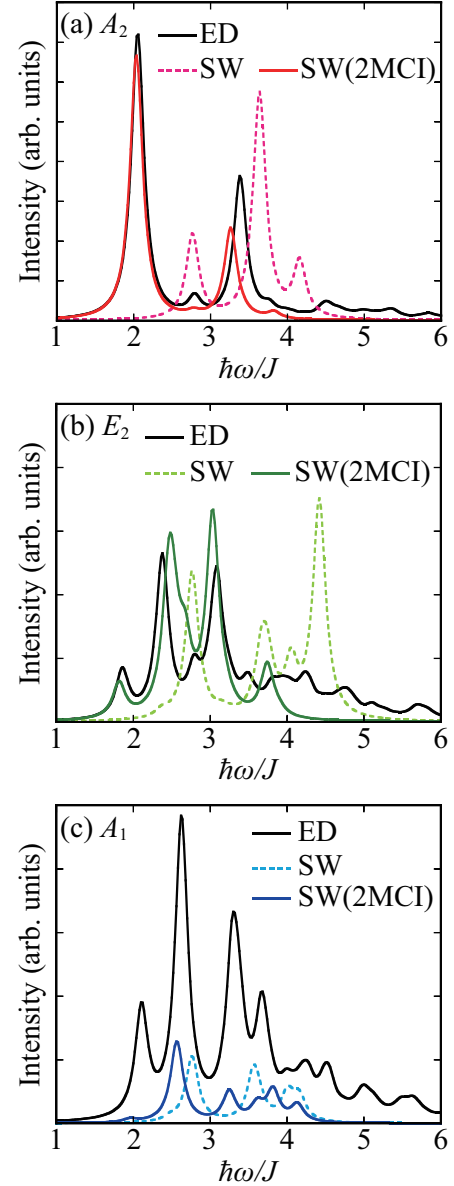


Figure 4 The fourth-order magnetic Raman spectra on the $N = 16$ sites cluster for (a) A_2 mode, (b) E_2 mode, and (c) A_1 mode. Spectra are calculated by Lanczös exact diagonalization (ED), spin-wave theory without magnon-magnon interactions (SW), and spin-wave theory with magnon-magnon interactions introduced by two-magnon excitation CI method [SW(2MCI)].

Coefficients $c_{0,n}$ and $c_{(k,l),n}$ are obtained by diagonalization of the CI Hamiltonian matrix:

$$H_{CI} = \begin{bmatrix} \langle 0M | H_{SW} | 0M \rangle & \langle 0M | H_{SW} | 2M \rangle \\ \langle 2M | H_{SW} | 0M \rangle & \langle 2M | H_{SW} | 2M \rangle \end{bmatrix} \quad (22)$$

We note that the two-magnon excitation CI calculation corresponds to solving the ladder-approximation Bethe-

Salpeter equation with interactions of the quartic magnon terms [12].

Results are shown in Fig. 4. First, we focus on the A_2 mode spectra [Fig. 4(a)]. Comparing the both spin-wave results, Raman peaks soften down after considering the magnon-magnon interactions. The line shape and peak positions of the result of the interacting spin-wave are in good agreement with result of the exact diagonalization. We conclude that the spin-wave calculation of the two-magnon scattering process can describe the spin-chirality-driven A_2 mode magnetic Raman spectrum very well.

For the E_2 mode spectra [Fig. 4(b)], the two-magnon scattering intensity of the spin-wave theory with the magnon-magnon interactions agrees with the exact result at low-frequency (about $\hbar\omega < 4J$) part. However, the interacting spin-wave result lacks high-frequency tail of the exact result, which is expected higher-order contributions.

On the other hand, from Fig. 4(c), the A_1 mode magnetic Raman spectra of the exact diagonalization and spin-waves disagree. The two-magnon scattering spin-wave spectra are quite smaller than the exact spectrum, even if it includes the magnon-magnon interactions. This suggests that the higher order multimagnon scattering, for instance four-magnon scattering, is dominant in the A_1 mode Raman intensity.

5 Conclusion

We have presented the magnetic Raman spectra of the two-dimensional C_{5v} Penrose lattice Heisenberg antiferromagnets. The Raman intensity within the Loudon-Fleury mechanism comes from the E_2 representation and shows no linear polarization dependence due to the degeneracy of the two-dimensional irreducible representation E_2 . In contrast, the fourth-order Raman operator yields spectral weights of A_1 and A_2 , as well as E_2 , representations and therefore exhibit strong polarization dependence in the Raman intensities beyond the Loudon-Fleury mechanism. The A_2 mode spectrum is driven by scalar-spin-chirality terms, and it is arisen from quasiperiodic structure of the Penrose lattice. We can separately extract every irreducible representation from the observation with the use of two linearly and one circularly polarized lights. The two-magnon scattering with the magnon-magnon interactions can describe the A_2 and E_2 mode spectra very well. This means that the spin-chirality excitations and exchange excitations can be mainly understood by the two-magnon scattering process. In contrast, the A_1 mode spectrum, which is almost caused by the ring-exchange excitations, disagree with the two-magnon scattering result. To understand the A_1 mode Raman spectrum, we have to consider the multimagnon scattering process, which is left for further investigation.

Acknowledgements We would like to thank J. Ohara and Y. Noriki for useful discussions. This study was supported by the Ministry of Education, Culture, Sports, Science, and Technology of Japan.

Appendix

In this section, we shall present the details of the fourth-order magnetic Raman operator. It is obtained by a fourth-order perturbation:

$$\mathcal{R}^{(4)} = \mathcal{P} H_c \frac{1}{\varepsilon_i - H_U} H_t \frac{1}{\varepsilon_i - H_U} H_t \frac{1}{\varepsilon_i - H_U} H_c \mathcal{P}$$

where H_c is the current operator, H_t is the electron transfer operator, and H_U is the on-site Coulomb repulsion operator, respectively. ε_i is the energy of the initial state. We fix that the initial states are direct product of singly-occupied electron states with incident photon, and the intermediate states are one holon and one doublon states with no photons. Under this condition, $(\varepsilon_i - H_U)^{-1} = (\hbar\omega_{\text{in}} - U)^{-1}$ becomes a c -number. \mathcal{P} is the projection operator which converts electron operators into spin-1/2 operators.

The fourth-order effective magnetic Raman operator is written as

$$\begin{aligned} \mathcal{R}^{(4)} = & \sum_{\langle 1,2,3,4 \rangle} \frac{t^4}{(U - \hbar\omega_{\text{in}})^3} \left\{ \right. \\ & - 4 \sum_{n=1}^4 (e_{\text{in}} \cdot \delta_n) (e_{\text{sc}}^* \cdot [\delta_{n+1} + 2\delta_{n+2} + \delta_{n+3}]) \\ & \times [\mathcal{Q}_{1234} + \mathcal{Q}_{1432} - \mathcal{Q}_{1324}] \\ & + 2i \sum_{n=1}^4 \Delta_n^{\text{ch}} \mathbf{S}_{n+2} \cdot (\mathbf{S}_{n+1} \times \mathbf{S}_n) \\ & + \sum_{n=1}^4 \Delta_n^{\text{ex}} \mathbf{S}_n \cdot \mathbf{S}_{n+1} + \sum_{n=1}^2 \Delta_n^{\text{ex}'} \mathbf{S}_n \cdot \mathbf{S}_{n+2} \left. \right\} \\ & + \sum_{\langle 1,2,3 \rangle} \frac{t^4}{(U - \hbar\omega_{\text{in}})^3} \left\{ \right. \\ & 4i [(e_{\text{in}} \cdot \delta_1) (e_{\text{sc}}^* \cdot \delta_2) - (e_{\text{in}} \cdot \delta_2) (e_{\text{sc}}^* \cdot \delta_1)] \\ & \times \mathbf{S}_3 \cdot (\mathbf{S}_2 \times \mathbf{S}_1) \\ & + 2 \sum_{n=1}^2 \tilde{\Delta}_n^{\text{ex}} \mathbf{S}_n \cdot \mathbf{S}_{n+1} \\ & - 2 [(e_{\text{in}} \cdot \delta_1) (e_{\text{sc}}^* \cdot \delta_2) + (e_{\text{in}} \cdot \delta_2) (e_{\text{sc}}^* \cdot \delta_1)] \\ & \times \mathbf{S}_1 \cdot \mathbf{S}_3 \left. \right\} \end{aligned}$$

$$\mathcal{Q}_{ijkl} \equiv (\mathbf{S}_i \cdot \mathbf{S}_j) (\mathbf{S}_k \cdot \mathbf{S}_l)$$

$$\begin{aligned} \Delta_n^{\text{ch}} \equiv & (e_{\text{in}} \cdot \delta_n) (e_{\text{sc}}^* \cdot [-\delta_{n+1} - 2\delta_{n+2} + \delta_{n+3}]) \\ & + (e_{\text{in}} \cdot \delta_{n+1}) (e_{\text{sc}}^* \cdot [-\delta_{n+2} + 2\delta_{n+3} + \delta_n]) \\ & + (e_{\text{in}} \cdot \delta_{n+2}) (e_{\text{sc}}^* \cdot [\delta_{n+3} + 2\delta_n + \delta_{n+1}]) \\ & + (e_{\text{in}} \cdot \delta_{n+3}) (e_{\text{sc}}^* \cdot [-\delta_n - 2\delta_{n+1} - \delta_{n+2}]) \end{aligned}$$

$$\begin{aligned}\Delta_n^{\text{ex}} \equiv & (e_{\text{in}} \cdot \delta_n)(e_{\text{sc}}^* \cdot [-\delta_{n+1} + 2\delta_{n+2} - \delta_{n+3}]) \\ & + (e_{\text{in}} \cdot \delta_{n+1})(e_{\text{sc}}^* \cdot [\delta_{n+2} - 2\delta_{n+3} - \delta_n]) \\ & + (e_{\text{in}} \cdot \delta_{n+2})(e_{\text{sc}}^* \cdot [\delta_{n+3} + 2\delta_n + \delta_{n+1}]) \\ & + (e_{\text{in}} \cdot \delta_{n+3})(e_{\text{sc}}^* \cdot [-\delta_n - 2\delta_{n+1} + \delta_{n+2}])\end{aligned}$$

$$\begin{aligned}\Delta_n^{\text{ex}'} \equiv & (e_{\text{in}} \cdot \delta_n)(e_{\text{sc}}^* \cdot [\delta_{n+1} + 2\delta_{n+2} - \delta_{n+3}]) \\ & + (e_{\text{in}} \cdot \delta_{n+1})(e_{\text{sc}}^* \cdot [-\delta_{n+2} + 2\delta_{n+3} + \delta_n]) \\ & + (e_{\text{in}} \cdot \delta_{n+2})(e_{\text{sc}}^* \cdot [\delta_{n+3} + 2\delta_n - \delta_{n+1}]) \\ & + (e_{\text{in}} \cdot \delta_{n+3})(e_{\text{sc}}^* \cdot [-\delta_n + 2\delta_{n+1} + \delta_{n+2}])\end{aligned}$$

$$\begin{aligned}\tilde{\Delta}_n^{\text{ex}} \equiv & (e_{\text{in}} \cdot \delta_n)(e_{\text{sc}}^* \cdot [\delta_1 + \delta_2]) \\ & + (e_{\text{in}} \cdot [\delta_1 + \delta_2])(e_{\text{sc}}^* \cdot \delta_n)\end{aligned}$$

where $\sum_{\langle 1,2,3,4 \rangle}$ is taken over four-sites loop pathways, and $\sum_{\langle 1,2,3 \rangle}$ is taken over three-sites linked pathways (see Fig. 5). e_{in} and e_{sc}^* are the polarization vectors of incident and scattered photons. $\delta_n \equiv r_{n+1} - r_n$ is the vector that connects site n to site $n + 1$. In these equations, we set $n \doteq n + 4$ as a modulus.

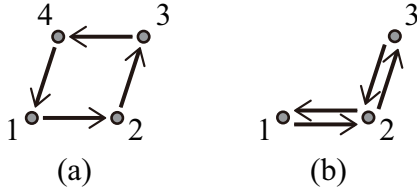


Figure 5 Two types of fourth-order-electron-hopping pathways. (a) Four-site loop pathway and (b) three-site pathway. Arrows indicate the movement of electrons arising from H_c and H_t .

References

- [1] D. Schechtman, I. Blech, D. Gratias, and J. W. Cahn, Phys. Rev. Lett. **53**, 1951 (1984).
- [2] M. Kohmoto and B. Sutherland, Phys. Rev. Lett. **56**, 2740 (1986).
- [3] M. Arai, T. Tokihiro, T. Fujiwara, and M. Kohmoto, Phys. Rev. B **38**, 1621.
- [4] N. Macé, A. Jagannathan, P. Kalugin, R. Mosseri, and F. Piéchon, Phys. Rev. B **96**, 045138 (2017).
- [5] K. Deguchi, S. Matsukawa, N. K. Sato, T. Hattori, K. Ishida, H. Takakura, and T. Ishimasa, Nat. Mater. **11**, 1013 (2012).
- [6] A. Koga and H. Tsunetsugu, Phys. Rev. B **96**, 214402 (2017).
- [7] Y. Okabe and K. Niizeki, J. Phys. Soc. Jpn. **57**, 16 (1988).
- [8] A. Szallas and A. Jagannathan, Phys. Rev. B **77**, 104427 (2008).
- [9] S. Wessel and I. Milat, Phys. Rev. B **71**, 104427 (2005).
- [10] P. A. Fleury and R. Loudon, Phys. Rev. **166**, 514 (1968).
- [11] S. Sugai, S. Shamoto, and M. Sato, Phys. Rev. B **38**, 6436 (1988).
- [12] C. M. Canali and S. M. Girvin, Phys. Rev. B **45**, 7127 (1992).
- [13] A. V. Chubukov and D. M. Frenkel, Phys. Rev. B **52**, 9760 (1995).
- [14] A. W. Sandvik, S. Capponi, D. Poilblanc, and E. Dagotto, Phys. Rev. B **57**, 8478 (1998).
- [15] N. B. Perkins, G.-W. Chern, and W. Brenig, Phys. Rev. B **87**, 174423 (2013).
- [16] O. Cépas, J. O. Haerter, and C. Lhuillier, Phys. Rev. B **77**, 172406 (2008).
- [17] B. S. Shastry and B. I. Shraiman, Phys. Rev. Lett. **65**, 1068 (1990).
- [18] B. S. Shastry and B. I. Shraiman, Int. J. Mod. Phys. B **5**, 365 (1991).
- [19] W.-H. Ko, Z.-X. Liu, T.-K. Ng, and P. A. Lee, Phys. Rev. B **81**, 024414 (2010).
- [20] F. Michaud, F. Vernay, and F. Mila, Phys. Rev. B **84**, 184424 (2011).